

Room Temperature Acceptorless Alkane Dehydrogenation from Molecular η^6 -Alkane Complexes

Alasdair I. McKay, Alexander J. Bukvic, Bengt E. Tegner, Arron L. Burnage, Antonio J. Martinez-Martinez, Nicholas H. Rees, Stuart A. Macgregor, and Andrew S. Weller

J. Am. Chem. Soc., **Just Accepted Manuscript** • DOI: 10.1021/jacs.9b05577 • Publication Date (Web): 27 Jun 2019

Downloaded from <http://pubs.acs.org> on June 27, 2019

Just Accepted

"Just Accepted" manuscripts have been peer-reviewed and accepted for publication. They are posted online prior to technical editing, formatting for publication and author proofing. The American Chemical Society provides "Just Accepted" as a service to the research community to expedite the dissemination of scientific material as soon as possible after acceptance. "Just Accepted" manuscripts appear in full in PDF format accompanied by an HTML abstract. "Just Accepted" manuscripts have been fully peer reviewed, but should not be considered the official version of record. They are citable by the Digital Object Identifier (DOI®). "Just Accepted" is an optional service offered to authors. Therefore, the "Just Accepted" Web site may not include all articles that will be published in the journal. After a manuscript is technically edited and formatted, it will be removed from the "Just Accepted" Web site and published as an ASAP article. Note that technical editing may introduce minor changes to the manuscript text and/or graphics which could affect content, and all legal disclaimers and ethical guidelines that apply to the journal pertain. ACS cannot be held responsible for errors or consequences arising from the use of information contained in these "Just Accepted" manuscripts.

Room Temperature Acceptorless Alkane Dehydrogenation from Molecular σ -Alkane Complexes

Alasdair I. McKay,^{1‡} Alexander J. Bukvic,^{1‡} Bengt E. Tegner,^{2‡} Arron L. Burnage,² Antonio J. Martinez-Martinez,¹ Nicholas H. Rees,¹ Stuart A. Macgregor,^{2*} Andrew S. Weller^{1*}

¹ Chemistry Research Laboratories, University of Oxford, Oxford OX1 3TA, United Kingdom. ² Institute of Chemical Sciences, Heriot Watt University, Edinburgh EH14 4AS, United Kingdom.

ABSTRACT: The industrially important non-oxidative catalytic dehydrogenation of light alkanes via C–H activation is a highly endothermic process that generally requires high temperatures and/or a sacrificial hydrogen acceptor to overcome unfavorable thermodynamics. This is complicated by alkanes being such poor ligands, meaning that binding at metal centers prior to C–H activation is disfavored. We demonstrate that by biasing the pre-equilibrium of alkane binding, by using solid-state molecular organometallic chemistry (SMOM-chem), well-defined isobutane and cyclohexane σ -complexes, $[\text{Rh}(\text{Cy}_2\text{PCH}_2\text{CH}_2\text{PCy}_2)(\eta\text{:}\eta\text{-(H}_3\text{C)CH(CH}_3)_2\text{) [BAR}^{\text{F}}_4\text{]}]$ and $[\text{Rh}(\text{Cy}_2\text{PCH}_2\text{CH}_2\text{PCy}_2)(\eta\text{:}\eta\text{-C}_6\text{H}_{12})\text{] [BAR}^{\text{F}}_4\text{]}$ can be prepared by simple hydrogenation in a solid/gas single-crystal to single-crystal transformation of precursor alkene complexes. Solid-gas H/D exchange with D_2 occurs at all C–H bonds in both complexes, pointing to a variety of low energy fluxional processes that occur for the bound alkane ligands in the solid-state. These are probed by variable temperature SSNMR experiments and periodic DFT calculations. These alkane σ -complexes undergo spontaneous acceptorless dehydrogenation at 298 K to reform the corresponding isobutene and cyclohexadiene complexes, by simple application of vacuum or Ar-flow to remove H_2 . These processes can be followed temporally, and modelled using classical chemical, or Johnson–Mehl–Avrami–Kologoromov (JMAK), kinetics. When per-deuteration is coupled with dehydrogenation of cyclohexane to cyclohexadiene, this allows for two successive KIEs to be determined [$k_{\text{H}}/k_{\text{D}} = 3.6(5)$ and $10.8(6)$], showing that the rate determining steps involve C–H activation. Periodic DFT calculations predict overall barriers of 20.6 kcal/mol and 24.4 kcal/mol for the two dehydrogenation steps, in good agreement with the values determined experimentally. The calculations also identify significant C–H bond elongation in both rate-limiting transition states and suggest that the large $k_{\text{H}}/k_{\text{D}}$ for the second dehydrogenation results from a pre-equilibrium involving C–H oxidative cleavage and a subsequent rate-limiting β -H transfer step.

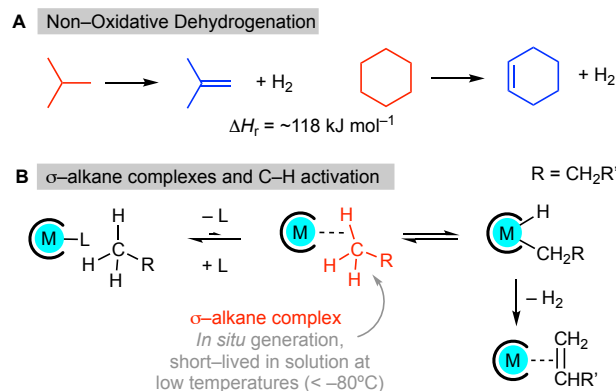
INTRODUCTION

The “on-purpose” non-oxidative catalytic dehydrogenation of abundant, unreactive and low value light alkanes to produce alkenes, which are key chemical intermediates, is of significant industrial importance,^{1,2} that is amplified by the recent movement in feedstocks from naphtha to shale gas. Dehydrogenation is an energy intensive process, due to the high positive enthalpy of reaction (e.g. isobutane, cyclohexane: $\Delta H_r^\circ \sim 118 \text{ kJ mol}^{-1}$, Scheme 1A),³ and high temperatures are thus required to drive the reaction (commonly 550–750 °C using a heterogeneous catalyst) which present challenges for catalyst decomposition, coking and process selectivity.⁴ In molecular homogenous dehydrogenation systems a sacrificial alkene H_2 -acceptor is commonly used at operating temperatures of 120–200 °C,^{5–7} or lower with more exotic acceptors.⁸ In the absence of an acceptor dehydrogenation can be driven photolytically,^{9–11} or by continuous removal of H_2 at elevated temperatures (~ 150 °C) to bias the thermodynamics.^{12–14}

Key, but undetected, first-formed intermediates in both homogeneously and heterogeneously catalyzed alkane dehydrogenation are σ -alkane complexes, in which the C–H bond of an alkane interacts with the metal center, in a 3-center 2-electron σ -interaction, prior to C–H oxidative bond cleavage and β -hydrogen elimination (Scheme 1B).^{15–18} As C–H bonds in alkanes are strong, non-polar and relatively sterically crowded, alkanes are very poor ligands ($\text{M} \cdots \text{H}-\text{C}$ bond enthalpies less than 60 kJ mol^{-1}), meaning that such complexes have generally only

been observed using low temperature in situ (-80 °C or lower) NMR^{19–22} or in situ diffraction techniques,²³ or on very short timescales (μs to s) using Time Resolved Infrared experiments (TRIR).^{24–26} An additional challenge for catalytic alkane dehydrogenation is thus one of pre-equilibrium prior to C–H

Scheme 1. (A) Non-Oxidative Dehydrogenation of cyclohexane and isobutane. (B) σ -alkane complexes: pre-equilibrium, C–H oxidative cleavage and dehydrogenation; L = ligand and or solvent.

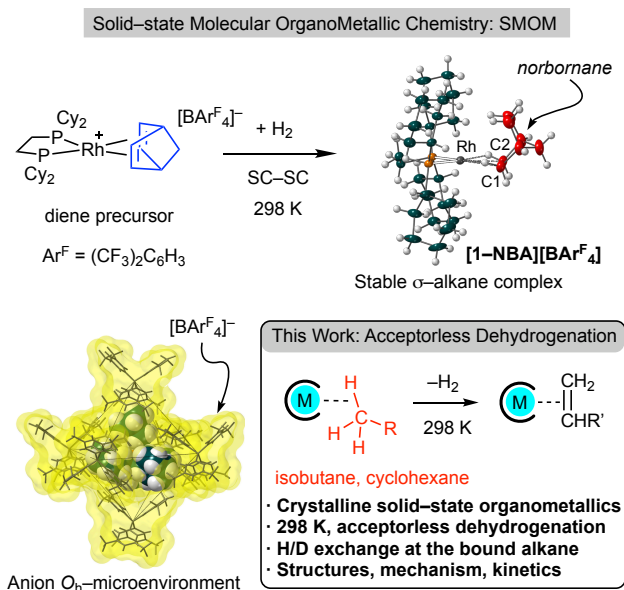


activation, as solvent or other ligands will generally outcompete any weak σ -interaction from the alkane under normal condi-

tions.^{21,27–31} However, C–H activation can be a rather facile process once a σ -complex is formed.^{7,26,32–34} Combined, all these factors make observing intermolecular dehydrogenation processes directly from σ -alkane complexes very challenging, and many experimental contributions have thus focused on the overall thermodynamics and catalytic efficiencies of such processes, as well as kinetic studies of catalytic systems, including isotopic-substitution.^{5,35} Such work has also been supported by numerous computational studies.^{25,36,37}

We have recently reported that σ -alkane complexes can be prepared using so-called solid-state molecular organometallic (SMOM) chemistry techniques. By operating under single-crystal to single-crystal conditions (SC–SC),³⁸ addition of H₂ to precursor norbornadiene complexes, e.g. [Rh(R₂PCH₂CH₂PR₂)($\eta^2\eta^2$ -C₇H₈)]([BAR^F₄]) (R = ⁱPr, Cy, Cyp; Ar^F = 3,5-(CF₃)₂C₆H₃) generates the corresponding σ -alkane (i.e. norbornane) complexes directly in the solid-state. Some of these show remarkable stability at room temperature, which we postulate is due to the, albeit non-porous, octahedral nanoreactor³⁹ environment provided by the [BAR^F₄][–] anions (Scheme 2, R = Cy, [1-NBA][BAR^F₄]).^{40–43}

Scheme 2 SMOM approach to the synthesis of stable σ -alkane complexes in the solid-state.



We now report that by using this methodology the synthesis of σ -complexes of the light alkanes cyclohexane and isobutane can be achieved at Rh(I) centers, that allow for their detailed characterization by single crystal X-ray diffraction, solid-state NMR (SSNMR) spectroscopy and periodic DFT calculations. These complexes are shown to undergo rapid H/D exchange at all the C–H bonds of the bound alkane on addition of D₂, and a remarkable acceptorless dehydrogenation at 25 °C by simple removal of H₂ under flow or vacuum, for which significant kinetic isotope effects can be directly measured for the dehydrogenation of cyclohexane. The products of dehydrogenation, cyclohexene and isobutene, are key intermediates in the chemical manufacturing chain (nylon production and gasoline additives/butyl rubber respectively).^{44,45} In particular isobutene is currently produced commercially using a high temperature non-oxidative dehydrogenation of isobutane (e.g. the Oleflex

process: heterogeneous Pt/Sn catalyst at 525–700 °C). Our results provide definitive structural and reactivity data for the key intermediates in both heterogenous and homogeneous catalytic dehydrogenation processes. They also demonstrate the potential for SMOM systems to mediate low temperature dehydrogenation by biasing both the pre-equilibrium towards σ -complexes, and the overall dehydrogenation by straightforward removal of H₂.

RESULTS AND DISCUSSION

Synthesis and Characterization of Isobutane and Cyclohexane σ -Alkane complexes. Alkene precursors to the σ -alkane complexes, namely isobutene [Rh(Cy₂PCH₂CH₂PCy₂)(C₄H₈)]([BAR^F₄]) [1-C₄H₈][BAR^F₄] and cyclohexadiene [Rh(Cy₂PCH₂CH₂PCy₂)(η^4 -C₆H₈)]([BAR^F₄]) [1-C₆H₈][BAR^F₄] were prepared in good yield as crystalline materials (Figure 1A).⁴⁶ While [1-C₆H₈][BAR^F₄] is prepared using traditional solution routes, [1-C₄H₈][BAR^F₄] is best accessed via SC–SC solid/gas reactivity by addition of gaseous isobutene to [1-NBA][BAR^F₄] and displacement of NBA,⁴⁷ followed by recrystallization from a solution saturated with isobutene. Single crystal X-ray diffraction, low temperature solution and SSNMR spectroscopy confirm the formulations as alkene complexes.⁴⁶ The solid-state structure of the isobutene complex [1-C₄H₈][BAR^F₄] has a bound alkene fragment that also has an additional supporting agostic Rh...H₃C interaction, and so features an $\eta^2_\pi:\eta^2_{C-H}$ -binding mode, similar to the recently reported propene analogue.⁴⁷ The isobutene is disordered over two superimposed positions that are related by a non-crystallographic apparent C₂ axis, which means that discussion of the detailed bond metrics is not appropriate. The cyclohexadiene complex,

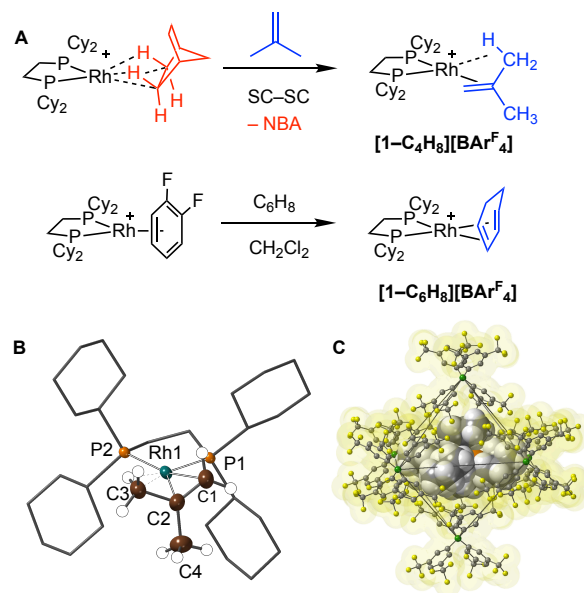
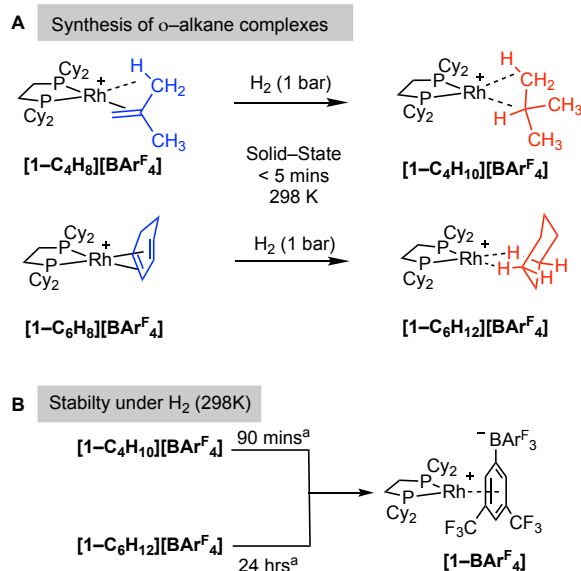


Figure 1. (A) Synthesis of [1-C₄H₈][BAR^F₄] and [1-C₆H₈][BAR^F₄]. (B) Solid-state structure of [1-C₄H₈][BAR^F₄]. Displacement ellipsoids shown at the 30% probability level. [BAR^F₄][–] anions and most hydrogen atoms omitted for clarity. One disordered component shown. Rh1–P1, 2.2238(9); Rh1–P2, 2.2400(9); Rh1–C1, 2.262(6); Rh1–C2, 2.136(8); Rh1–C3, 2.368(9); C1–C2, 1.320(12); C2–C3, 1.474(13), 1.513(13). (C) Packing diagram of [1-C₄H₈][BAR^F₄] (van der Waal radii) showing the O_h arrangement of [BAR^F₄][–] anions.

[1-C₆H₈][BAR^F₄] adopts the expected η^4 diene binding mode (Fig. S95). Both [1-C₄H₈][BAR^F₄] and [1-C₆H₈][BAR^F₄] have extended solid-state structures in which the organometallic cation is surrounded in a pseudo-*O_h* cavity defined by the [BAR^F₄]⁻ anions (Fig. S93,95).⁴⁶ and Figure 1C shows that for [1-C₄H₈][BAR^F₄], [1-C₄H₈][BAR^F₄] is a rare example of a crystallographically characterized isobutene complex.⁴⁸

Like its propene analogue,⁴⁷ the isobutene complex [1-C₄H₈][BAR^F₄] exhibits fluxional processes at 298 K in both solution and the solid-state that exchange the methyl and methylene hydrogens. This symmetry in the cation is demonstrated by a single environment being observed in the 298 K ³¹P{¹H} NMR solution spectrum [δ 95.3, d, J (RhP) = 179 Hz] while no distinct alkene resonances are observed in the ¹³C{¹H} NMR (solid-state or solution) or ¹H NMR spectra (solution). We propose a 1,3-shift via a methallyl hydride intermediate,⁴⁹ coupled with a further exchange of two methyl groups by libration. These can be slowed at low temperature, i.e. 183 K solution, 158 K solid-state. Thus, in solution two mutually coupled environments are now observed in the low temperature ³¹P{¹H} NMR spectrum at δ 97.6 [dd, J (RhP) = 201, J (PP) = 26 Hz], 93.6 [dd, J (RhP) 158, J (PP) = 26 Hz]. The ³¹P{¹H} SSNMR spectrum shows two overlapping environments centered at δ 94.8. The solution ¹³C{¹H} NMR spectrum shows two signals due to coordinated alkene [δ 111.5, 72.6], and the ¹H NMR spectrum shows a signal that can be assigned to the alkene groups and an agostic Rh...H₃C interaction [δ -0.15], although the low temperature limit was not reached (Figs. S1 to 7). The ¹³C{¹H} SSNMR spectrum shows alkene signals at δ 108.6 and 70.6. The agostic Rh...H₃C signal could not be unambiguously identified, but a resonance at δ 15.7 that is absent in the 298 K spectrum is consistent with such an interaction.⁴⁷ In contrast [1-C₆H₈][BAR^F₄] does not show fluxional behavior, and its NMR spectra are unremarkable.

Scheme 3. Synthesis and stability of [1-C₄H₁₀][BAR^F₄] and [1-C₆H₁₂][BAR^F₄]; ^a Time for ~10% decomposition in the solid-state under 1 atm H₂ (by ³¹P{¹H} SSNMR spectroscopy) = 15 minutes and 90 minutes respectively.



Addition of H₂ (298 K, 1 bar, 15 mins) to single crystalline samples of each of the alkene complexes resulted in rapid hydro-

genation of the alkene to form the corresponding σ -alkane complexes, [1-C₄H₁₀][BAR^F₄] and [1-C₆H₁₂][BAR^F₄], via SC-SC transformations, Scheme 3A, in which the *O_h* arrangement of [BAR^F₄]⁻ anions is retained (Fig. S94,96). Analysis of the isobutane σ -complex [1-C₄H₁₀][BAR^F₄] by single crystal X-ray diffraction (R = 9.5%, two independent molecules in the unit cell) shows the Rh(I)-center has two η^2 -Rh...H-C interactions⁴² from adjacent methyl (C1) and methine (C2) groups in the alkane [e.g. Rh...C1, 2.362(14); Rh...C2, 2.442(7) Å for one of the independent molecules in the unit cell], Figure 2. These distances are similar to those in [1-NBA][BAR^F₄] that also shows a 1,2- η^2 : η^2 -coordination motif,⁵⁰ albeit through two methylene groups [2.389(3), 2.400(3) Å].⁴¹ This description is also fully supported by electronic structure analyses (see Supporting Materials). The C-C distances in the alkane show single bonds [1.516(13)–1.551(13) Å]. The Rh-P distances in [1-C₄H₁₀][BAR^F₄] are shorter by ~0.04 Å than in [1-C₄H₈][BAR^F₄], reflecting the weaker *trans* influence of the alkane ligands. A chemically identical disordered component is related by a small rotation of the alkane (25°) around C2 (Fig. S94). Hydrogen atoms were placed in calculated positions in the final refinement. Addition of H₂ is also signaled by a change in geometry around the tertiary C-atom (C2) from sp² in [1-C₄H₈][BAR^F₄] to sp³ in [1-C₄H₁₀][BAR^F₄]: angles around C2 = 360.0° and 335.1° respectively. The ¹³C{¹H} SSNMR spectrum shows a featureless alkane region (δ 110–50), while in the ³¹P{¹H} SSNMR spectrum a major new broad signal is shifted 12 ppm to lower field compared to the starting alkene complex (δ 106.8). Notably, under these conditions a small amount of starting material and alkane-loss decomposition product in which the [BAR^F₄]⁻ anion is coordinated with the metal center, [1-BAR^F₄],⁴¹ are also observed (~10% total). Longer times for H₂ addition (90 mins, 298 K) resulted in complete loss of crystallinity to give [1-BAR^F₄],⁵¹ Scheme 3B, as measured by ³¹P{¹H} SSNMR spectroscopy.

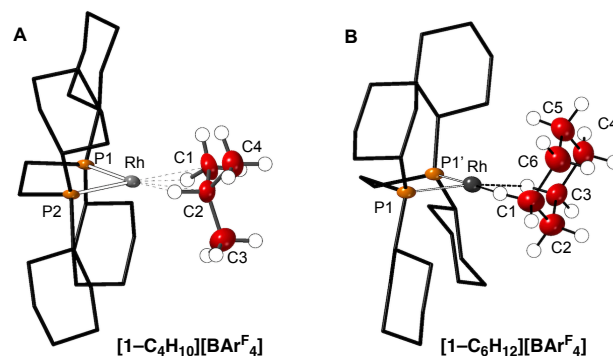


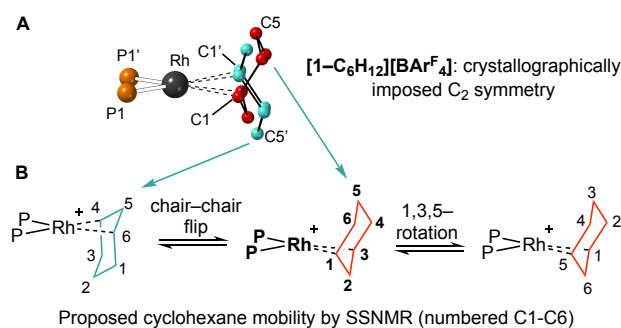
Figure 2. Solid-state structures of [1-C₄H₁₀][BAR^F₄] and [1-C₆H₁₂][BAR^F₄]. Displacement ellipsoids shown at the 30% probability level. [BAR^F₄]⁻ anions and most hydrogen atoms omitted for clarity. Only one disordered component shown. (A) [1-C₄H₁₀][BAR^F₄] (one of the independent cations): Rh1–P1, 2.1830(14); Rh1–P2, 2.1914(14); Rh1–C1, 2.362(14); Rh1–C2, 2.442(7); C1–C2, 1.551(13); C2–C3, 1.528(13); C2–C4, 1.516(13). (B) [1-C₆H₁₂][BAR^F₄]: Rh1–P1, 2.191(2); Rh1–C1, 2.62(2); Rh1–C3, 2.53(2); C1–C2, 1.529(15); C2–C3, 1.531(15).

For [1-C₆H₁₂][BAR^F₄] the cyclohexane ligand is disordered over two positions (Figure 2 and Scheme 4A), related by a crystallographically-imposed C₂ axis which, when coupled with the reduction in data quality inherent in SC-SC transformations (R

= 10.3%), meant that the C–C distances in the alkane were necessarily restrained. Nevertheless, the coordination geometry is fully consistent with a σ -alkane ligand interacting via two C–H \cdots Rh interactions in a 1,3-motif.⁵² The Rh \cdots C distances [2.62(2), 2.53(2) Å] are longer than in [1-C₄H₁₀][BAr^F₄], but similar to those in [1-pentane][BAr^F₄] [2.514(4), 2.522(5) Å] that also shows a 1,3-coordination mode for the alkane.⁵³ The ³¹P{¹H} and ¹³C{¹H} NMR spectra are consistent with this formulation, and are similar to [1-C₄H₁₀][BAr^F₄]. Notably C=C environments that are observed in the ¹³C{¹H} SSNMR spectrum of [1-C₆H₈][BAr^F₄] (96–81 ppm) disappear on addition of H₂ (Fig. S22, S25). Despite the longer Rh \cdots C distances, [1-C₆H₁₂][BAr^F₄] is significantly less sensitive to displacement by H₂ than [1-C₄H₁₀][BAr^F₄] and after 90 minutes under H₂ only 10% decomposition is observed by ³¹P{¹H} SSNMR (Scheme 3B and Fig. S34).⁵¹ This may reflect the weak, multiple, stabilizing dispersive interactions between the surface of cyclohexane and the proximal [BAr^F₄][−] in the anion–microenvironment as we have previously commented on for other alkane–complexes.⁴²

For both [1-C₄H₁₀][BAr^F₄] and [1-C₆H₁₂][BAr^F₄] addition of MeCN to the crystalline solids results in liberation of the free alkane as determined by ¹H NMR spectroscopy of the vacuum transferred volatiles. Neither [1-C₄H₁₀][BAr^F₄] or [1-C₆H₁₂][BAr^F₄] are stable in solution, and zwitterionic [1-BAr^F₄], [1-(CH₂Cl)₂][BAr^F₄]⁵⁴ and free alkane are observed by NMR spectroscopy on dissolving in cold (183 K) CD₂Cl₂. On warming these solutions decompose to give a mixture of products, as identified by ESI–MS, some of which come from C–Cl activation of the solvent.⁵⁵

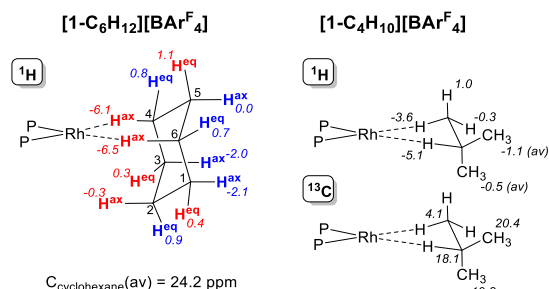
Scheme 4. (A) Crystallographically-imposed cyclohexane disorder in [1-C₆H₁₂][BAr^F₄]. (B) Proposed fluxional process in the solid-state.



The alkane ligands in both the σ -complexes undergo motion in the solid-state, as we have noted previously for the norbornane ligand in [1-NBA][BAr^F₄] and related systems.^{42,53,56} In the ¹H/¹³C HETCOR FSLG SSNMR⁵⁹ spectrum of [1-C₆H₁₂][BAr^F₄] at 158 K a distinct correlation is observed between $\delta(^{13}\text{C})$ 19.7 and two signals in the ¹H projection at δ −1.6/1.2, consistent with diastereotopic methylene groups in cyclohexane (i.e. axial and equatorial, Figs. S29–S32). At 198 K these signals disappear, suggesting the onset of a fluxional process. A 158 K ¹³C–NQS experiment, that probes motion of (CH₂)_n groups in a frequency range similar to or greater than the ¹H–¹³C dipolar coupling,⁵⁷ shows two signals at δ 21.4 and 19.7 that are assigned to the cyclohexane ligand. At 198 K only one signal is observed at δ 21.4 (Figs. S27,28). These observations, combined with the disorder in the single-crystal X-ray structure, lead us to propose a combination of two low energy fluxional processes are occurring: a 1,3,5–ring walk, that operates

at 158 K, retains the fidelity of the diastereotopic methylene groups and does not exchange 1,3,5 and 2,4,6 positions; and a higher energy chair–chair ring flip that makes all the carbon positions equivalent (Scheme 4B). This latter fluxional process mirrors the observed disorder in the solid-state structure. Low energy fluxional processes in the solid-state have been reported for other σ -alkane, or related, complexes.^{42,53,56} While these two processes make all the carbon environments equivalent on the NMR timescale, they do not exchange all the axial and equatorial C–H groups in the ring, and this model for the fluxional process leads to six C–H bonds that contact the metal center (highlighted in red, Scheme 5) and another set of six C–H bonds of the cyclohexane ligand that are always remote from the metal (blue). SSNMR calculations (periodic-DFT, GIPAW method) on the nearest-neighbor ion-pair derived from the optimized structure of [1-C₆H₁₂][BAr^F₄] reveal significant high field shifts for the C₄–H_{ax} and C₆–H_{ax} hydrogens that interact directly with the metal center,^{20,21,41,56} with smaller high field shifts computed for the remote C₁–H_{ax} and C₃–H_{ax} positions. The latter are likely due to ring current effects from the nearby⁵⁸ anion aryl groups (Fig. S33).⁴¹ The computed average chemical shift for the H_{ax} and H_{eq} hydrogen at the C₂, C₄ and C₆ positions is −4.3 ppm and 0.8 ppm, respectively, in reasonable agreement with the values observed at 158 K.

Scheme 5. Computed chemical shifts for [1-C₆H₁₂][BAr^F₄] and [1-C₄H₁₀][BAr^F₄].

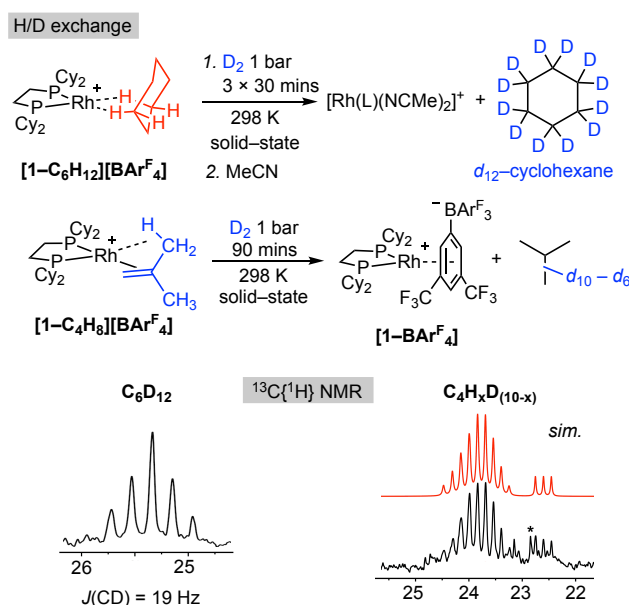


For the isobutane ligand in [1-C₄H₁₀][BAr^F₄] two environments are observed in the 203 K NQS spectrum in the aliphatic region, at δ ~21 and ~15. At 158 K these signals disappear, suggesting an arrested low energy motion for the isobutane ligand in the solid-state. A ¹H/¹³C HETCOR FSLG SSNMR experiment at 158 K shows a correlation between the signal at δ ~21 (¹³C) and δ −3.4 (¹H projection), similar to [1-C₆H₁₂][BAr^F₄], signaling a Rh \cdots H–C interaction (Figs. S11–13). However, these experimental data do not map directly onto computed chemical shift averages for [1-C₄H₁₀][BAr^F₄] (Scheme 5). Given our recent success in calibrating computational and experimentally determined chemical shifts in σ -alkane complexes in the solid-state^{53,56} this discrepancy may point to a fluxional/equilibrium process that is occurring at low temperature that remains to be determined.

Short-lived, cyclic and branched σ -alkane complexes have been characterized in solution at low temperature (173 K or lower) by in situ NMR spectroscopy, e.g. (η^5 -C₅H₅)Re(CO)₂(cyclohexane)⁶⁰ and (η^5 -C₅H₅)Mn(CO)₂(isopentane),⁶¹ or TRIR experiments, (η^5 -C₅H₅)Rh(CO)(cycloalkane).⁶² In such species the alkanes bind with the metal centers through M \cdots H–C interactions in an ensemble of interconverting isomers, and similar to that postulated to occur for cyclohexane here, these interconvert by chain or ring walking, or axial/equatorial isomerization.

H/D exchange in σ -alkane complexes. The isolation of $[1-C_4H_{10}][BAR^F_4]$ and $[1-C_6H_{12}][BAR^F_4]$ in the solid-state in synthetically meaningful amounts (up to 0.15 g) offers an opportunity to study C–H activation processes in σ -alkane complexes in the absence of competing pre-equilibria. Catalytic H/D exchange in alkanes using D_2 probes such processes by reversibly intercepting the corresponding metal-alkyl hydride intermediate that arises from C–H bond cleavage (Scheme 1B).³⁰ We have recently shown that $[1-NBA][BAR^F_4]$ undergoes a remarkably selective *exo*-H/D exchange at the bound alkane on addition of D_2 in a solid/gas SC–SC reaction.⁵⁶ Addition of D_2 (298 K) to either $[1-C_4H_{10}][BAR^F_4]$ or $[1-C_6H_{12}][BAR^F_4]$ results in relatively rapid H/D exchange at *all* the C–H bonds of the bound alkane. This is best shown for crystalline $[1-C_6H_{12}][BAR^F_4]$, where 3 successive additions of D_2 results in perdeuteration of the cyclohexane (optimized, 90 minutes total, 10% decomposition). This is conveniently measured by liberating the alkane on addition of MeCN to the crystalline solid (Scheme 6). GC–MS analysis shows the formation of only one isotopologue, C_6D_{12} ($m/z = 96.17$), confirmed by the $^{13}C\{^1H\}$ NMR spectrum, which shows a quintet [δ 25.3; $J(CD) = 19$ Hz], and the 2H NMR spectrum that shows a single environment for cyclohexane at δ 1.37. Shorter exposure times (3×5 minutes) resulted in a mixture of isotopologues for which D-incorporation increases monotonically, as measured by GC–MS (Fig. S48). Interestingly, despite the shorter reaction times, the isotopologue distribution is dominated by 6-fold H/D exchange (i.e. $C_6H_6D_6$) and above. As the perdeuteration observed indicates all 12 C–H bonds are involved in H/D exchange an additional fluxional process that exchanges the faces of the cyclohexane under conditions of exogenous D_2 is necessary that, in combination with the 1,3,5-ring walk/chair–chair flip already described (Scheme 4), allows the metal center to access to all the methylene C–H positions. The distribution of isotopologues at short exposure times suggests this face exchange process is likely higher in energy than the other two process (1,3,5-rotation and chair–chair flip). These processes have been defined computationally, see later.

Scheme 6. H/D exchange in the σ -alkane complexes, and associated $^{13}C\{^1H\}$ NMR (and simulated) spectra of the liberated alkane. * = pentane impurity.



For $[1-C_4H_{10}][BAR^F_4]$ the limited stability of the isobutane σ -alkane complex under H_2 (D_2) meant that H/D exchange experiments started from the isobutene complex for experimental expediency. This formed a mixture of isobutane isotopologues, $C_4H_xD_{(10-x)}$ ($x = 0 - 4$, Fig. S41), after 90 minutes, as measured by GC–MS of the volatiles after vacuum transfer into CD_2Cl_2 . This distribution of isotopologues also increases monotonically. Beyond this time complete decomposition by loss of alkane occurs to form $[1-BAR^F_4]$. The $^{13}C\{^1H\}$ NMR spectrum of volatiles liberated on addition of MeCN shows that H/D incorporation at both methine (C–H) and methyl (CH_3) groups under the timescale of the experiment, the former signaled by the observation of an apparent 1:1:1 triplet [δ , 22.5; $J(CD) = 20$ Hz, Fig. 3]. Initial deuteration of isobutene places D in this position.⁶³ The methyl groups present a more complicated set of overlapping resonances that have been simulated with $CD_3/CD_2H/CDH_2$ in a 62:30:8 ratio (Scheme 6). Two environments in a relative 1:9 ratio [δ 1.86, 0.85] are observed in the 2H NMR spectrum, and are assigned to the *d*-methine and *d*-methyl respectively (Fig. S39). Again, there must be a fluxional process in the solid-state that allows for all the C–H bonds of the methyl groups to undergo H/D exchange, however decomposition of the alkane complex under D_2 (H_2) atmosphere makes studying this less straightforward than for its cyclohexane analog. Nevertheless the rotational disorder observed in the solid-state structure of $[1-C_4H_{10}][BAR^F_4]$, coupled with the mobility suggested by NQS experiments and deuteration levels approaching C_4D_{10} , indicates that all methyl groups can contact the Rh-center.

For both cyclohexane and isobutane σ -alkane complexes stepwise H/D exchange with D_2 could occur either by oxidative addition of D_2 followed by σ -CAM⁶⁴ with a $Rh \cdots H-C$ bond, or via oxidative cleavage of an alkane C–H bond to form $Rh-H$ species that are intercepted by D_2 . The alternative pairwise exchange would involve dehydrogenation to form an alkene which is then deuterated, as we and others have commented upon previously.^{21,56} While the monotonic increase in partially deuterated isotopologues for both alkanes suggests stepwise exchange, as we show next alkane dehydrogenation is a remarkably facile process, and thus we cannot rule out either mechanism – or if both operate contemporaneously. Computational studies are underway to probe the precise mechanism of H/D exchange and will be reported in a future contribution.

Acceptorless dehydrogenation of σ -alkane complexes. In the absence of H_2 or D_2 , acceptorless dehydrogenation of the bound σ -alkane ligand occurs in the solid-state to reform the corresponding alkene complex. Although for both free isobutane and cyclohexane this is an endothermic process – and this remains the case when these are bound to a metal center (see computational section) – removal of the generated H_2 results in a remarkably fast (minutes to hours) dehydrogenation in the solid-state to reform the alkene complexes (Figure 3). This process is so facile that isolated $[1-C_4H_{10}][BAR^F_4]$ and $[1-C_6H_{12}][BAR^F_4]$, and their deuterated analogues, show measurable dehydrogenation under an Ar atmosphere after only 5 minutes at 298 K. Isolation of pure $[1-C_4H_{10}][BAR^F_4]$, especially, is finely balanced: under an H_2 (or D_2) atmosphere complete alkane loss occurs over 90 minutes to form $[1-BAR^F_4]$ while under Ar, or mild vacuum (10^{-2} mbar), dehydrogenation occurs on a comparable timescale. $[1-C_6H_{12}][BAR^F_4]$ is more robust to alkane loss, meaning the dehydrogenation process is more reliably followed.

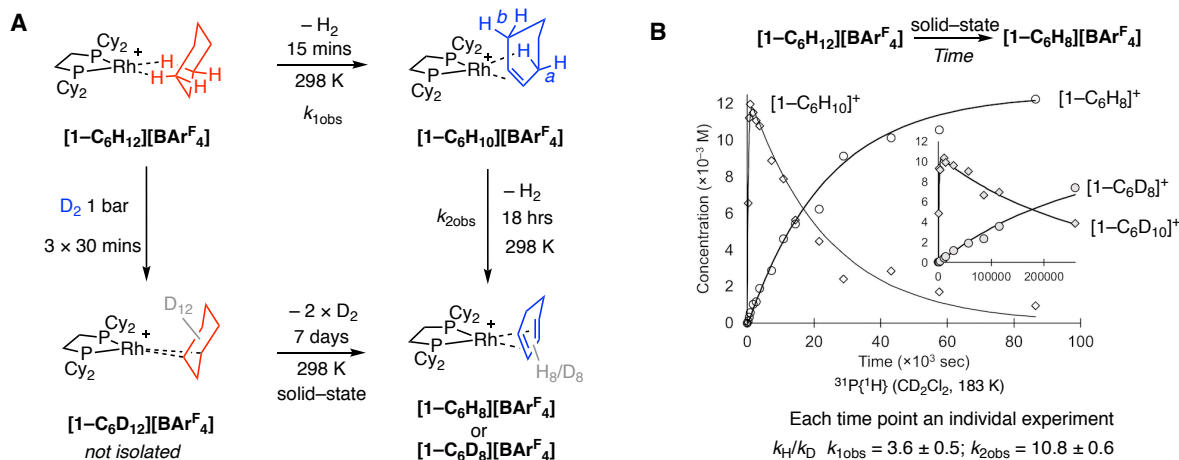


Figure 3. (A) Dehydrogenation of crystalline $[1-C_6H_{12}][BARF_4]$ or in situ formed $[1-C_6D_{12}][BARF_4]$ under Ar flow or vacuum (10^{-2} mbar). (B) Temporal plot of the solid-state dehydrogenation under vacuum, as measured by quantitative $^{31}P\{^1H\}$ NMR spectroscopy of dissolved sample (CD_2Cl_2 , 183 K). Signals due to $[1-(CH_2Cl)_n][BARF_4]$ are taken as a proxy for $[1-C_6H_{12}][BARF_4]$ (not shown). Each time point is an individual experiment, calibrated to an internal standard of PPh_3 of known concentration in a flame-sealed capillary (d_6 -acetone). Solid-lines are simulated plots (COPASI⁶⁵) for two consecutive first order processes. Inset shows dehydrogenation of $[1-C_6D_{12}][BARF_4]$.

The dehydrogenation of $[1-C_6H_{12}][BARF_4]$ can be monitored by solid-state and solution NMR spectroscopies by running multiple solid-state experiments in which the time of reaction is varied before dissolving in CD_2Cl_2 at 183 K by vacuum transfer of solvent onto the sample. For consistency, finely-ground microcrystalline powder was used (10 mg), a dynamic vacuum was applied (10^{-2} mbar) to remove H_2 and low temperature (183 K, CD_2Cl_2 , internal standard) quantitative $^{31}P\{^1H\}$ NMR spectroscopy of the dissolved samples was deployed to track progress. Under these low temperature measurement conditions the alkane complexes form the solvent adducts, $[1-(CH_2Cl)_n][BARF_4]$, alongside $[1-BARF_4]$, both of which act as a proxy for the σ -alkane complexes.⁴⁷ For $[1-C_6H_{12}][BARF_4]$ these experiments show complete dehydrogenation to the diene $[1-C_6H_8][BARF_4]$ in 16 hrs, which was fully characterized by solution NMR spectroscopy.⁴⁶ The dehydrogenation can also be tracked using in situ $^{31}P\{^1H\}$ and $^{13}C\{^1H\}$ SSNMR spectroscopy (Fig. S67-S68), but as long-range order is lost in the process, likely due to crystal cracking,⁶⁶ attempts to follow this by SC-SC X-ray diffraction experiments were not successful. The material does retain microcrystallinity, however,^{67,68} as demonstrated by a powder X-ray diffraction experiment on the dehydrogenated sample.

This temporal profile shows that after 15 minutes the principal component (~95%) is a new complex that can be fully characterized using low temperature solution NMR spectroscopy (183 K) to be the result of a single dehydrogenation, i.e. the cyclohexene complex $[1-C_6H_{10}][BARF_4]$. Addition of $CO(g)$ in a solid/gas reaction after 15 minutes displaces the cyclohexene allowing for full characterization by NMR spectroscopy and GC/MS (Fig. S79-S82). By analogy with other mono-alkene complexes we propose the cyclohexene in $[1-C_6H_{10}][BARF_4]$ adopts an $\eta^2\pi:\eta^2C-H$ binding mode in which the π -interaction is supported by a agostic interaction from an adjacent methylene group. This structure is also located computationally (see below). Notable data include two mutually coupled environments in the $^{31}P\{^1H\}$ spectrum [δ 98.0, $J(RhP) = 207$ Hz; δ 91.5, $J(RhP) = 159$ Hz], while in the 1H NMR spectrum a single alkene environment is observed (2H, δ 5.23, confirmed by

HSQC) and a resonance in the high field region of the 1H NMR spectrum characteristic of a $Rh \cdots H-C$ agostic interaction (2H, δ -1.01). We propose a low energy libration of the alkene to account for this C_s symmetry observed in solution that exchanges C_a and C_b (Figure 3 and S69), as has been proposed for the closely associated $[1-(cis-2-butene)][BARF_4]$ analogue where the calculated barrier to libration is 3 kcalmol⁻¹.⁴⁷ Warming solutions resulted in decomposition to $[1-C_6H_8][BARF_4]$, the benzene complex $[1-C_6H_6][BARF_4]$ (independently synthesized) and $[1-BARF_4]$.

The corresponding perdeuterated analogue, $[1-C_6D_{12}][BARF_4]$, also undergoes dedeuteriation in the solid-state, but much more slowly, taking 7 days to afford $[1-C_6D_8][BARF_4]$, as shown by ESI-MS, 1H , 2H and $^{31}P\{^1H\}$ solution NMR spectra (Figure 3). In the $^{13}C\{^1H\}$ NMR spectrum three environments are observed at δ 94.7 [1:1:1 triplet, $J(CD) = 26$ Hz], δ 82.3 [1:1:1 triplet, $J(CD) = 23$ Hz], δ 21.3 [1:2:3:2:1 quintet, $J(CD) \sim 20$ Hz] assigned to the two pairs of $=CD$ and CD_2 groups respectively (Fig. S87). That the bound, deuterated, diene is also seen after addition of D_2 to $[1-C_6H_{12}][BARF_4]$, shows that the σ -alkane interactions must persist on H/D exchange prior to undergoing dehydrogenation.

By using a solution-based kinetics model the temporal evolution of the dehydrogenation of $[1-C_6H_{12}][BARF_4]$ to give first $[1-C_6H_{10}][BARF_4]$ and then $[1-C_6H_8][BARF_4]$ in the solid-state as measured by the individual trapping experiments can be simulated, using COPASI,⁶⁵ by two consecutive first-order processes with $k_{1obs} = 3.1(2) \times 10^{-3} s^{-1}$ and $k_{2obs} = 4.2(2) \times 10^{-5} s^{-1}$.⁶⁹ These correspond to ΔG^\ddagger (298 K) of 21 and 24 kcalmol⁻¹ respectively for these two overall C-H activation processes. Dedeuteriation from the – not isolated – perdeuterated σ -alkane complex $[1-C_6D_{12}][BARF_4]$ can also be modelled by two (slower) first order processes, and this allows for a significant kinetic isotope effect (KIE) to be determined for these two overall dehydrogenation processes: KIE (k_{1obs}) = 3.6(5) and KIE (k_{2obs}) = 10.8(6). The first dehydrogenation (k_{1obs}) has a KIE similar to other cyclohexane mono-dehydrogenations, e.g. photo-dehydrogenation using *trans*-Rh(PMe₃)₂(CO)Cl ($k_H/k_D = 5.3$)⁹ and photo- or transfer-dehydrogenation using

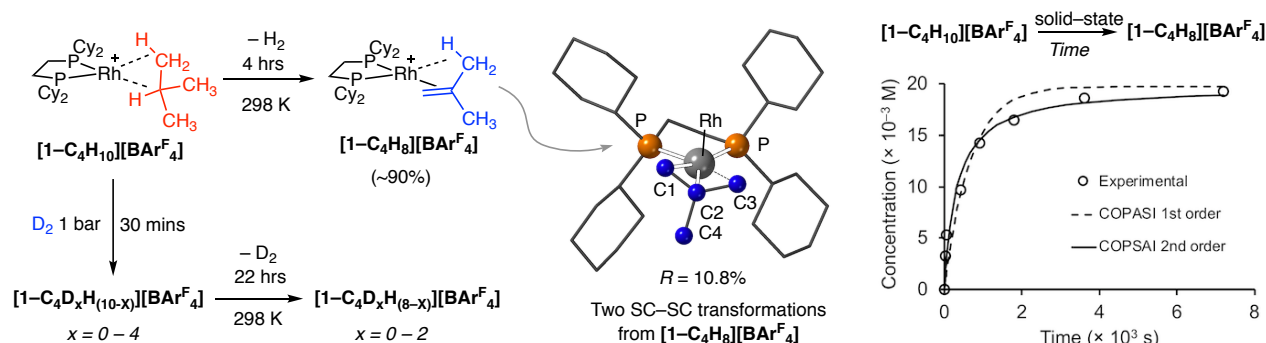


Figure 4. Dehydrogenation of crystalline $[1-C_4H_{10}][BARF_4]$ under Ar flow or vacuum (10^{-2} mbar). Solid-state structure of $[1-C_4H_8][BARF_4]$ formed in a SC-SC transformation (ball and stick). Temporal plot of the solid-state dehydrogenation under vacuum. Details as in Figure 4. Lines are simulated plots (COPASI⁶⁵) for first order process (dashed), second order process (solid).

$Ir(PR_3)_2(H)_2(O_2CF_3)$ ($k_H/k_D = 4.4-7.7$).⁶ The second dehydrogenation of the cyclohexene shows a larger kinetic isotope effect. While this may indicate a small tunnelling contribution, similarly large KIEs have been reported for photochemically promoted C-H activations at $Cp^*Rh(CO)_2$,^{26,33} or C-H activation of methane in $Cp^*_2ScCH_2CMe_3$.⁷⁰ The details of these dehydrogenation mechanisms are discussed in the computational study.

A remarkably straightforward dehydrogenation process also occurs from the isobutane complex $[1-C_4H_{10}][BARF_4]$, so that after 4 hours complete H_2 loss has occurred in the solid-state to give $[1-C_4H_8][BARF_4]$ (Figure 4). This occurs under a mild dynamic vacuum (10^{-2} mbar), as for the cyclohexane analogue, and can be followed using solution trapping or solid-state NMR spectroscopy. This provides data suitable for a quantitative analysis, by measuring the concentrations of $[1-C_4H_8][BARF_4]$ for different samples where the time of dehydrogenation is varied. This also occurs in an Ar-flow, resulting in a similar temporal profile. Unlike for $[1-C_6H_{12}][BARF_4]$ this SC-SC process retains enough long-range order to confirm the structure of the isobutene complex by single crystal X-ray diffraction, and this is essentially identical to that prepared independently (see earlier), albeit with a poorer structural solution ($R = 10.8\%$, twinned crystals), Figure 4. Surprisingly to us, this dehydrogenation process is best modelled as following overall second order kinetics (i.e. second order in $[1-C_4H_{10}][BARF_4]$), $k_{(obs)} = 1.6(2) \times 10^{-4} M^{-1}s^{-1}$, and Figure 4 shows a COPASI modelled fit to both 1st and 2nd order processes. The same process occurs from partially deuterated $[1-C_4D_xH_{(10-x)}][BARF_4]$, formed from

30 mins addition of D_2 to $[1-C_4H_{10}][BARF_4]$, to give $[1-C_4D_xH_{(8-x)}][BARF_4]$ ($x = 0-4$). This partial deuteration meant that experiments to determine a KIE were not attempted.

The dehydrogenation of these σ -alkane complexes in the solid-state has also been modelled using modified Johnson-Mehl-Avrami-Kolmogorov (JMAK) kinetics,⁷¹⁻⁷³ that express the progress (i.e. conversion) of solid-state reactions in terms of a nucleation and growth model (Equation 1, Figure 5): where k is the growth rate constant and n is the Avrami exponent. Exponents close to $n = 4, 3$ and 2 are suggestive of 3-D, 2-D and 1-D growth, respectively, while $n = 1$ is indicative of a non-cooperative transformation that occurs throughout the crystal, and can be related to a classical first order process in homogenous systems.⁷⁴ Pertinently, JMAK analysis has been used to describe SC-SC photoreactions in the solid-state,⁷⁵⁻⁷⁷ while Finke has discussed the relationship between solid-phase reaction progress and classical chemical kinetics, especially the connections between k/n and rate constants/order in reaction.⁷³ Given the small number of data points for the first rapid dehydrogenation of $[1-C_6H_{12}][BARF_4]$, only the second dehydrogenation was modelled using JMAK reaction kinetics, and this yielded $n = 1.02(3)$ with an associated growth rate constant, k , of $4.2(2) \times 10^{-5} s^{-1}$ which is also an excellent fit with that determined using classical chemical kinetics (Figure 5, k_{2obs}), i.e. first order. We interpret this as each lattice point in the crystalline material acting independently for this second dehydrogenation step. For isobutane dehydrogenation in $[1-C_4H_{10}][BARF_4]$, different solid-state kinetics are determined: $n = 0.55(3)$ with an associated growth rate constant, k , of $1.6(6) \times 10^{-3} s^{-1}$ – which is not directly relatable to a classical rate constant given that $n \neq 1$.⁷⁴ It has been suggested that such non-integer Avrami constants point to the kinetics being diffusion controlled.⁷² It is interesting to note that this process can also be modelled using 2nd-order classical kinetics (vide supra), which may point to a cooperative process for H_2 loss in the single-crystal. While we currently are reluctant to overinterpret these observations, they could be related to a reaction front (i.e. H_2 loss) that moves through the crystal from outside to in, as we have previously demonstrated empirically by CO addition to an analogue of $[1-C_6H_8][BARF_4]$.⁷⁸ Differences in the second⁶⁹ dehydrogenation process between $[1-C_6H_{12}][BARF_4]$ ($n = 1$) and $[1-C_4H_{10}][BARF_4]$ ($n \sim 0.5$) may be related to the loss of long-range order in the former on dehydrogenation, likely via crystal degradation that exposes new crystal surfaces,⁶⁶ that may result in H_2 loss processes being less important to reaction progress.

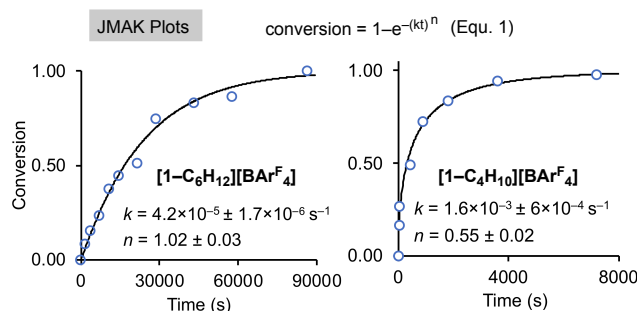


Figure 5. Modified JMAK plot⁷¹ of conversion versus time for the second dehydrogenation of $[1-C_6H_{12}][BARF_4]$ and dehydrogenation of $[1-C_4H_{10}][BARF_4]$. k = growth rate constant, n = Avrami exponent. Details as in Figure 3.

Computational Studies. Thermodynamics and Mechanism of Dehydrogenation. The thermodynamics of H₂ loss from [1-C₆H₁₂][BARF₄], [1-C₆H₁₀][BARF₄] and [1-C₄H₁₀][BARF₄] were computed with periodic DFT calculations with the PBE-D3 functional. Extended solid-state structures were fully optimized in all cases based on experimental crystallographic data, with the exception of [1-C₆H₁₀][BARF₄] where an initial geometry was constructed from [1-C₆H₁₂][BARF₄] via removal of H₂ from each cyclohexane ligand whilst maintaining the space group symmetry.⁷⁹ Optimized geometries for [1-C₆H₁₂][BARF₄] and [1-C₄H₁₀][BARF₄] provided good agreement with the experimental structures and, moreover, showed lengthening of the C–H bonds in contact with Rh (to 1.14 – 1.16 Å) that is consistent with σ-complex formation. This was also confirmed by electronic structure analyses (see Supporting Materials).⁵⁰ Including the solid-state environment in these calculations is essential. For example, optimizations on the isolated [1-C₆H₁₂]⁺ cation show cyclohexane to prefer a 1,2-binding mode in which it lies parallel to the Rh coordination plane, while in the solid-state this structure is strongly disfavored (see Fig. 9 and the discussion below). In [1-C₆H₁₀][BARF₄] the cyclohexene ligand binds to the Rh center in an η²:π:η²-C–H mode consistent with the NMR data measured for this species.

Figure 6 shows the computed free energies for dehydrogenation expressed both in terms of ΔG, the free energy change for dehydrogenation of a complete unit cell, and ΔG^{Rh}, the average free energy loss per Rh center (i.e. ΔG/Z). ΔG^{Rh} = +6.3 kcal/mol for [1-C₆H₁₂][BARF₄] and +6.7 kcal/mol for [1-C₆H₁₀][BARF₄].

Thus both dehydrogenation processes are endergonic, but still accessible thermodynamically upon removing H₂ from the system.

For the mechanisms of the sequential dehydrogenations of [1-C₆H₁₂][BARF₄] the experimental KIE data clearly signal significant C–H bond extension in the rate-determining steps for H₂ loss, however, they do not allow us to discriminate between C–H oxidative cleavage or β–H transfer as being rate limiting. Periodic DFT calculations were therefore employed to construct free energy profiles for these processes. These calculations used our previously published protocol,⁵⁶ i.e. for [1-C₆H₁₂][BARF₄] dehydrogenation at one of the Rh cations within the unit cell is considered while the remaining cell contents were free to relax within a unit cell that was constrained at its experimental dimensions.

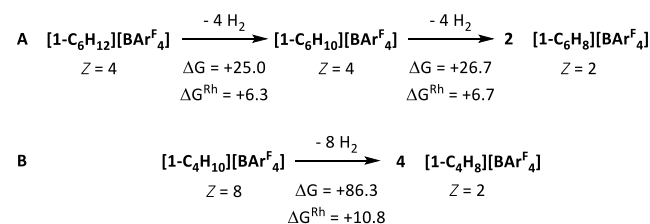


Figure 6. Computed thermodynamics of H₂ loss (kcal/mol) from (A) [1-C₆H₁₂][BARF₄] and (B) [1-C₄H₁₀][BARF₄] expressed as ΔG, the overall free energy change per unit cell, and ΔG^{Rh}, the free energy change per Rh center. See Supporting Materials for a comparison of computed and observed metrics.

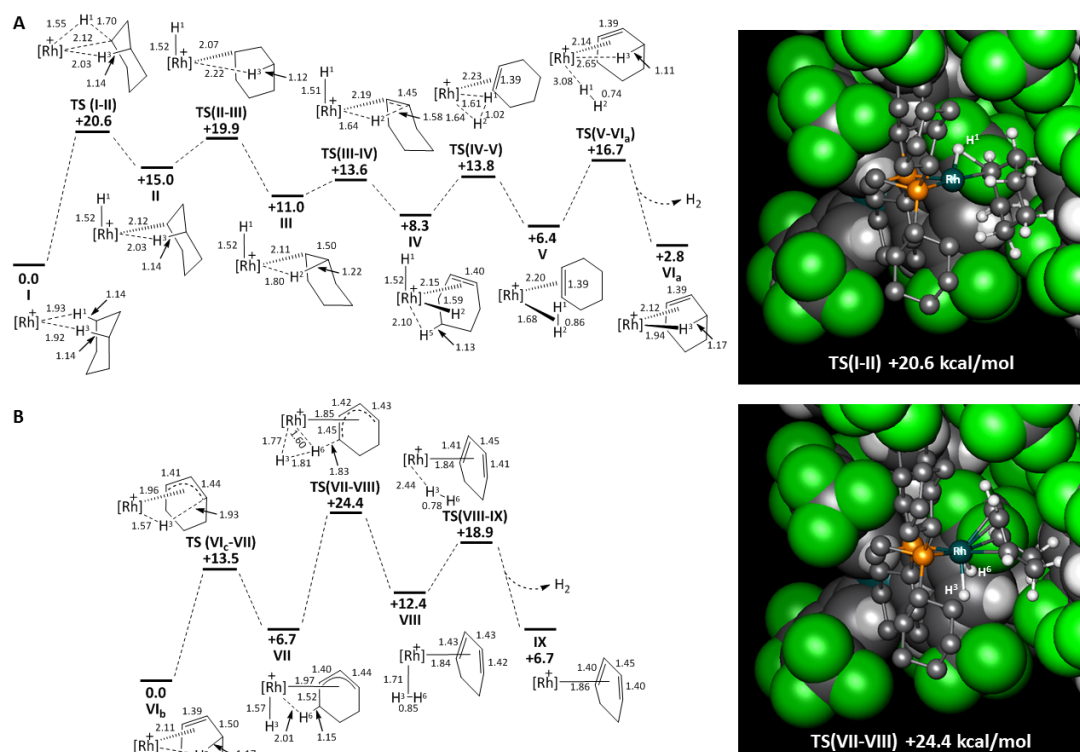


Figure 7. Free energy profiles (kcal/mol) for the dehydrogenation of (A) cyclohexane at one Rh center within the [1-C₆H₁₂][BARF₄] unit cell and (B) cyclohexene at one Rh center within the [1-C₆H₁₀][BARF₄] unit cell. Selected distances (Å) within the reacting Rh cations are shown, where [Rh]⁺ = [(Cy₂P(CH₂)₂PCy₂)Rh]⁺ and the remaining cell contents are omitted for clarity. Distances to delocalized π-ligands are to the centroid of the carbons involved. Also shown are the computed structures of the rate-limiting transition states for each profile, with the reacting Rh cation (ball and stick mode) set against the nearby unit cell contents (space-filling mode): Rh (teal); P (orange); C (charcoal); H (silver) and F (green).

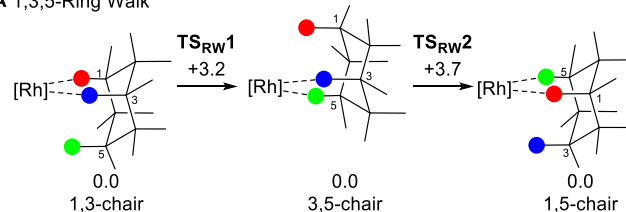
Figure 7A shows the computed free energy profile for dehydrogenation in $[1-C_6H_{12}][BAR^F_4]$, denoted **I** in the computational study. This commences with oxidative cleavage of the C–H¹ bond via **TS(I-II)** at +20.6 kcal/mol to give the hydrido alkyl intermediate **II** at +15.0 kcal/mol.⁸⁰ A facile rearrangement then brings the C–H² bond into contact with the Rh center (**III**, +11.0 kcal/mol) and permits β -H transfer via **TS(III-IV)** at +13.6 kcal/mol. This forms the Rh(III) dihydride intermediate **IV** at +8.3 kcal/mol in which the cyclohexene engages in an additional agostic interaction via the C–H⁵ bond. H–H reductive coupling then provides η^2 -H₂ complex **V** from which H₂ dissociates via **TS(V-VI_a)** at +16.7 kcal/mol to give the cyclohexene adduct **VI_a** which, once H₂ molecule is removed from the lattice,⁸¹ has a free energy of +2.8 kcal/mol.⁸² The overall dehydrogenation barrier of 20.6 kcal/mol agrees well with the value derived from experiment (21 kcal/mol) and the rate limiting transition state features a C \cdots H¹ distance of 1.70 Å that is consistent with a significant k_H/k_D KIE.⁸⁰ The computed structure of **TS(I-II)** (Figure 7A, right) also highlights the proximity of the $[BAR^F_4]$ anion within the solid-state environment and indeed this and other stationary points along the profile all exhibit a number of H \cdots F contacts below the sum of the van der Waals radii (2.7 Å). A comparison of the solid-state profile in Figure 7A with that computed with the isolated cation (see Figure S97–S104) reveals several important differences. In the latter, facile rearrangement to more stable alternative 1,2-bis σ -cyclohexane complexes is computed from which C–H oxidative cleavage can proceed through a transition state at +9.7 kcal/mol. With this model the final H₂ loss becomes rate-limiting with $\Delta G^{\ddagger}_{span} = +19.6$ kcal/mol. Thus, although the overall barrier is reasonable, a simple molecular model fails to account for the observed KIE and even predicts the wrong geometry for the alkane complex (see also the discussion of cyclohexane rearrangements in Figure 9).

Figure 7B shows the equivalent free energy profile for the dehydrogenation of cyclohexene in the full $[1-C_6H_{10}][BAR^F_4]$ unit cell. Starting from this species (denoted **VI_b**), initial C–H³ bond activation forms allyl hydride **VII** at +6.7 kcal/mol which features an *exo*-orientation of the allyl ligand (i.e, with the central C–H oriented away from the Rh–H bond).⁸³ This allows the C–H⁶ bond to engage in an agostic interaction *cis* the Rh–hydride and so permits H-transfer via a σ -CAM mechanism to form η^2 -H₂ cyclohexadiene species **VIII** at +12.4 kcal/mol. H₂ dissociation and expulsion from the lattice forms **IX** at +6.7 kcal/mol. The overall barrier to dehydrogenation is 24.4 kcal/mol via **TS(VIII-IX)** and so provides excellent agreement with the activation barrier derived from experiment (24 kcal/mol). **TS(VIII-IX)** again exhibits significant C–H bond elongation (C–H⁶ = 1.83 Å), but in this case this rate determining transition state is preceded by a pre-equilibrium involving reversible C–H oxidative cleavage. We therefore suggest that the observed large isotope effect of 10.8 ± 0.6 arises from a combination of an equilibrium isotope effect and a KIE. A similar scenario has been offered for the isotope effect measured in photochemically-driven cyclohexane dehydrogenation using *trans*-Rh(PMe₃)₂(CO)Cl.⁹

Calculations also probed the fluxional processes involving the cyclohexane ligand in $[1-C_6H_{12}][BAR^F_4]$. The most accessible of these involves exchange of the three axial sites interacting with Rh via a 1,3,5-‘ring walk’ process and occurs with a very low barrier of 3.7 kcal/mol (see Figure 8A). This rotation also involves movement of the cyclohexane ring relative to the Rh

coordination such that the intermediate 3,5-chair structure (coincidentally at 0.0 kcal/mol) has the cyclohexane moiety oriented as seen in the second disordered component defined crystallographically (although note that in this calculation only one of the four Rh centers is accessing this geometry). To higher energy is a ‘ring flip’ process by which the axial and equatorial hydrogens on one face of the cyclohexane are exchanged. This proceeds through a twist-boat bis- σ -complex at +5.7 kcal/mol that is bound through the C–H³ and C–H⁶ bonds; this reflects a coupling of the half-chair transition state with a counter-clockwise rotation of the cyclohexane moiety. From this intermediate a further half-chair transition state can be located that retrieves a chair conformation and establishes a Rh–H⁴–C σ -interaction. This entails a clockwise rotation and again moves the cyclohexane above the Rh coordination plane⁸⁴ to the ‘disordered’ structure.

A 1,3,5-Ring Walk



B Ring Flip (axial-equatorial exchange)

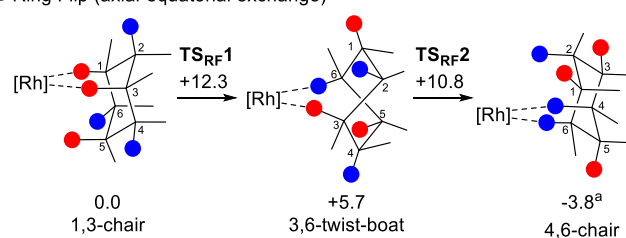


Figure 8. Computed pathways for cyclohexane rearrangements in $[1-C_6H_{12}][BAR^F_4]$ via (A) 1,3,5-Ring Walk and (B) Ring Flip mechanisms, with free energies indicated in kcal/mol. ^a The SCF electronic energy of this 4,6-chair structure places it 0.7 kcal/mol above the 1,3-chair, however a large entropic stabilization gives this anomalously low free energy.⁸⁰

Finally a mechanism for exchanging all 12 C–H positions was investigated, as required by the observation of per-deuterated C₆D₁₂ experimentally. This requires a ‘face-flip’ process whereby the set of six C–H bonds accessible via the 1,3,5-ring walk and ring flip processes are exchanged with the six C–H bonds that are initially remote from the metal center. In principle this could proceed via initial formation of a 1,2-bis σ -complex featuring Rh \cdots H^{eq}–C² Rh \cdots H^{ax}–C¹ interactions followed by rotation around the C¹–C² vector (see upper pathway, Figure 9). Such a process is readily accessible when computed in the isolated cation, however in the solid state none of these structures is a minimum and attempts to compute the central bis equatorial σ -complex gave energies at least 30 kcal/mol above the 1,3-reactant. This reflects the proximity of the $[BAR^F_4]$ anion in the solid state that does not permit the perpendicular orientation of the cyclohexane demanded by this pathway and again emphasizes the importance of taking the full solid-state environment into account when modelling these SMOM systems.

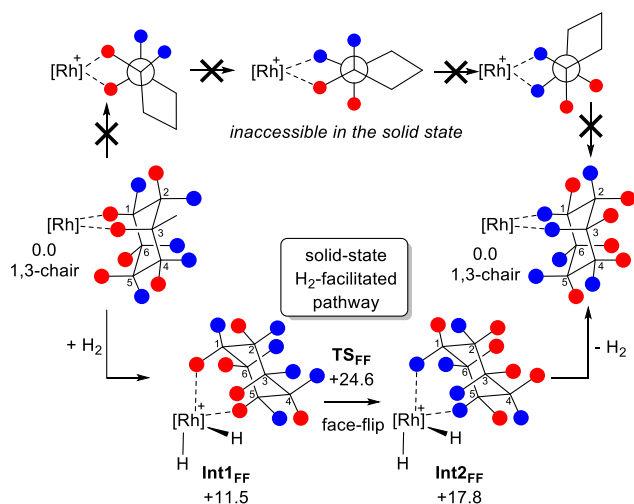


Figure 9. Pathways for the cyclohexane face-flip in $[1\text{-C}_6\text{H}_{12}][\text{BAR}^{\text{F}}_4]$. The upper pathway shows potential 1,2-bis σ -intermediates as Newman projections looking down the $\text{C}^2\text{-C}^1$ bond but which proved inaccessible in the solid-state. The lower pathway shows the proposed H_2 -facilitated pathway with free energies in kcal/mol. See text for details.

Instead we found that a face-flip process could be accessed upon addition and oxidative cleavage of H_2 . The resultant Rh(III) dihydride intermediates allows more flexibility for cyclohexane movement including access to additional σ -interactions in the axial sites (see lower pathway, Figure 9). The face-flip transition state, TS_{FF} , again involves rotation about the $\text{C}^1\text{-C}^2$ vector, but now that the ligand can access space above the Rh coordination plane this proves to be accessible within the solid-state pocket and proceeds with an overall computed barrier of 24.6 kcal/mol. Thus access to the remote ('blue') face of the cyclohexane ligand has a considerably higher barrier than rearrangements between the closer ('red') C-H bonds and this is consistent (assuming facile H/D exchange mechanisms) with the very rapid formation of $\text{C}_6\text{H}_6\text{D}_6$ upon exposure of $[1\text{-C}_6\text{H}_{12}][\text{BAR}^{\text{F}}_4]$ to D_2 , but the somewhat slower rate of formation of the higher $\text{C}_6\text{H}_x\text{D}_{(12-x)}$ isotopologues ($x = 0\text{-}5$).

CONCLUSIONS

We report here the industrially relevant, low temperature, acceptorless, dehydrogenation of the light alkanes isobutane and cyclohexane when bound as σ -complexes to a Rh(I) center. This demonstrates the advantages of solid-state organometallic chemistry (SMOM-chem) for the synthesis, characterization and subsequent reactivity of well-defined σ -complexes. Such species are traditionally short-lived when synthesized using *in situ* solution techniques at very low temperature, due to facile displacement of the weakly bound alkane by solvent or other exogenous ligand,^{60,61} making onward exploration of structure and reactivity very challenging. It is, without doubt, the micro-environment provided by the $[\text{BAR}^{\text{F}}_4]^-$ anions in the solid-state that allows for this chemistry of $\text{M}\cdots\text{H-C}$ alkane interactions described here to be developed.

By biasing the pre-equilibrium completely to the side of alkane binding in the solid-state, a number of important observations can be made. Experiment and computation show that both alkane ligands can access low energy fluxional processes in the solid-state that allow all the C-H bonds to come into contact with the metal center. This, in turn, permits per-deuteration by

H/D exchange using D_2 , indicating that C-H oxidative cleavage of the bound alkane must also be a relatively low energy process. When followed by β -H-elimination alkane dehydrogenation occurs – an overall endothermic process that normally requires very high temperatures, or (at lower temperatures) a sacrificial acceptor. The SMOM approach thus promotes both (i) alkane complex formation and (ii) the easy removal of liberated H_2 by simple application of vacuum or Ar-flow: two consecutive processes that are necessary for the observed reactivity. With the cyclohexane σ -complex dehydrogenation occurs via a cyclohexene intermediate to give the corresponding cyclohexadiene product. Coupling these dehydrogenations with prior per-deuteration allows for $k_{\text{H}}/k_{\text{D}}$ KIEs of 3.6(5) and 10.8(6), respectively, to be determined. Periodic DFT calculations identify rate-limiting C-H oxidative cleavage (for cyclohexane dehydrogenation) and β -H transfer (for cyclohexene dehydrogenation). The large KIE of the latter arises from the combination of significant C-H bond elongation in rate-limiting transition state with a pre-equilibrium that also involves C-H oxidative cleavage. The importance of solid-state computational studies, that capture the holistic microenvironment, compared with those on an isolated cation (i.e. so-called ‘gas phase’) is reflected by the excellent agreement between computation and experiment in probing the rate-limiting step – which are not captured in the absence of the solid-state environment.

While driving catalytic (acceptorless) dehydrogenation by removal of H_2 ,¹³ working in the solid-phase,⁸⁵ or under continuous-flow gas phase conditions at high temperatures,⁸⁶ are not new concepts, that stoichiometric dehydrogenation occurs at such well-defined σ -alkane complexes in the solid-state at 25 °C suggests opportunities to develop this process catalytically at lower temperatures. Fine-tuning of metal ligand coordination environment in the single-crystalline phase,⁴² coupled with the possibilities offered by expediently removing H_2 , offer potential solutions to move from stoichiometric to catalytic regimes in the single-crystalline state. Encouraging this approach we have recently shown that SMOM-systems are highly effective solid/gas alkene-isomerization catalysts.⁴⁷ Overcoming the acknowledged problems of product (alkene) inhibition,⁵ and understanding how gaseous reagents/products move in and out of the non-porous crystalline lattice are future challenges that we are currently focused on resolving.

ASSOCIATED CONTENT

Supporting Information

Full details of experimental methods, characterization data, details of computational methods and experiments and single crystal X-ray diffraction collection and refinement data. This material is available free of charge via the Internet at <http://pubs.acs.org>.

AUTHOR INFORMATION

Corresponding Author

andrew.weller@chem.ox.ac.uk
S.A.Macgregor@hw.ac.uk

Author Contributions

‡These authors contributed equally.

ACKNOWLEDGMENT

We thank the EPSRC (EP/M024210, EP/K035908, EP/K035681), the Leverhulme Trust (RPG-2015-447) and SCG Chemicals Co.,

Ltd, Thailand for funding. This work used the ARCHER UK National Supercomputing Service (<http://www.archer.ac.uk>) and the Cirrus UK National Tier-2 HPC Service at EPCC (<http://www.cirrus.ac.uk>) funded by the University of Edinburgh and EPSRC (EP/P020267/1). We thank Dr Graham Tizzard (UK National Crystallographic Service) for data collection on [1-C₆H₈][BARF₄], and Dr Hamish Yeung for valuable discussions in solid-state kinetics.

REFERENCES

- (1) Goldberg, K. I.; Goldman, A. S. Large-Scale Selective Functionalization of Alkanes. *Acc. Chem. Res.* **2017**, *50*, 620-626.
- (2) Sattler, J. J. H. B.; Ruiz-Martinez, J.; Santillan-Jimenez, E.; Weckhuysen, B. M. Catalytic Dehydrogenation of Light Alkanes on Metals and Metal Oxides. *Chem. Rev.* **2014**, *114*, 10613-10653.
- (3) *Nist Chemistry Webbook, Nist Standard Reference Database Number 69*, ; Linstrom, P. J.; Mallard, W. G., Eds.; National Institute of Standards and Technology: Gaithersburg MD, 20899, <https://doi.org/10.18434/T4D303>, (retrieved November 23, 2018).
- (4) Searles, K.; Chan, K. W.; Mendes Burak, J. A.; Zemlyanov, D.; Safonova, O.; Copéret, C. Highly Productive Propane Dehydrogenation Catalyst Using Silica-Supported Ga-Pt Nanoparticles Generated from Single-Sites. *J. Am. Chem. Soc.* **2018**, *140*, 11674-11679.
- (5) Kumar, A.; Bhatti, T. M.; Goldman, A. S. Dehydrogenation of Alkanes and Aliphatic Groups by Pincer-Ligated Metal Complexes. *Chem. Rev.* **2017**, *117*, 12357-12384.
- (6) Burk, M. J.; Crabtree, R. H. Selective Catalytic Dehydrogenation of Alkanes to Alkenes. *J. Am. Chem. Soc.* **1987**, *109*, 8025-8032.
- (7) Zhou, X.; Malakar, S.; Zhou, T.; Murugesan, S.; Huang, C.; Emge, T. J.; Krogh-Jespersen, K.; Goldman, A. S. Catalytic Alkane Transfer Dehydrogenation by PSP-Pincer-Ligated Ruthenium. Deactivation of an Extremely Reactive Fragment by Formation of Allyl Hydride Complexes. *ACS Cat.* **2019**, *9*, 4072-4083.
- (8) Solowey, D. P.; Mane, M. V.; Kurogi, T.; Carroll, P. J.; Manor, B. C.; Baik, M.-H.; Mindiola, D. J. A New and Selective Cycle for Dehydrogenation of Linear and Cyclic Alkanes under Mild Conditions Using a Base Metal. *Nat. Chem.* **2017**, *9*, 1126.
- (9) Maguire, J. A.; Boese, W. T.; Goldman, A. S. Photochemical Dehydrogenation of Alkanes Catalyzed by Trans-Carbonylchlorobis(trimethylphosphine)Rhodium: Aspects of Selectivity and Mechanism. *J. Am. Chem. Soc.* **1989**, *111*, 7088-7093.
- (10) Chowdhury, A. D.; Julis, J.; Grabow, K.; Hannebauer, B.; Bentrup, U.; Adam, M.; Franke, R.; Jackstell, R.; Beller, M. Photocatalytic Acceptorless Alkane Dehydrogenation: Scope, Mechanism, and Conquering Deactivation with Carbon Dioxide. *ChemSusChem* **2014**, *8*, 323-330.
- (11) Rábay, B.; Braun, T.; Falkenhagen, J. P. Photolytic C-H Activation and Dehydrogenation of Alkanes at Cyclopentadienyl Iridium Complexes in a Perfluorinated Solvent. *Dalton Trans.* **2013**, *42*, 8058-8065.
- (12) Xu, W.-W.; P. Rosini, G.; Krogh-Jespersen, K.; S. Goldman, A.; Gupta, M.; M. Jensen, C.; C. Kaska, W. Thermochemical Alkane Dehydrogenation Catalyzed in Solution without the Use of a Hydrogen Acceptor. *Chem. Commun.* **1997**, 2273-2274.
- (13) Aoki, T.; Crabtree, R. H. Homogeneous Tungsten, Rhenium, and Iridium Catalysts in Alkane Dehydrogenation Driven by Reflux of Substrate or of Cosolvent or by Inert-Gas Flow. *Organometallics* **1993**, *12*, 294-298.
- (14) Zhu, K.; Achord, P. D.; Zhang, X.; Krogh-Jespersen, K.; Goldman, A. S. Highly Effective Pincer-Ligated Iridium Catalysts for Alkane Dehydrogenation. DFT Calculations of Relevant Thermodynamic, Kinetic, and Spectroscopic Properties. *J. Am. Chem. Soc.* **2004**, *126*, 13044-13053.
- (15) Hartwig, J. F. *Organotransition Metal Chemistry*; University Science Books: Sausalito, USA, 2010.
- (16) Weller, A. S.; Chadwick, F. M.; McKay, A. I. Transition Metal Alkane-Sigma Complexes. *Adv. Organomet. Chem.* **2016**, *66*, 223-276.
- (17) Bergman, R. G. C-H Activation. *Nature* **2007**, *446*, 391.
- (18) Zhu, Q.; Wang, G.; Liu, J.; Su, L.; Li, C. Effect of Sn on Isobutane Dehydrogenation Performance of Ni/SiO₂ Catalyst: Adsorption Modes and Adsorption Energies of Isobutane and Isobutene. *ACS App. Mat. Interface.* **2017**, *9*, 30711-30721.
- (19) Calladine, J. A.; Duckett, S. B.; George, M. W.; Matthews, S. L.; Perutz, R. N.; Torres, O.; Vuong, K. Q. Manganese Alkane Complexes: An IR and NMR Spectroscopic Investigation. *J. Am. Chem. Soc.* **2011**, *133*, 2303-2310.
- (20) Bernskoetter, W. H.; Schauer, C. K.; Goldberg, K. I.; Brookhart, M. Characterization of a Rhodium(I)-Methane Complex in Solution. *Science* **2009**, *326*, 553-556.
- (21) Walter, M. D.; White, P. S.; Schauer, C. K.; Brookhart, M. Stability and Dynamic Processes in 16ve Iridium(III) Ethyl Hydride and Rhodium(I) σ -Ethane Complexes: Experimental and Computational Studies. *J. Am. Chem. Soc.* **2013**, *135*, 15933-15947.
- (22) Yau, H. M.; McKay, A. I.; Hesse, H.; Xu, R.; He, M.; Holt, C. E.; Ball, G. E. Observation of Cationic Transition Metal-Alkane Complexes with Moderate Stability in Hydrofluorocarbon Solution. *J. Am. Chem. Soc.* **2016**, *138*, 281-288.
- (23) Gonzalez, M. I.; Mason, J. A.; Bloch, E. D.; Teat, S. J.; Gagnon, K. J.; Morrison, G. Y.; Queen, W. L.; Long, J. R. Structural Characterization of Framework-Gas Interactions in the Metal-Organic Framework Co₂(Dobdc) by in Situ Single-Crystal X-Ray Diffraction. *Chem. Sci.* **2017**, *8*, 4387-4398.
- (24) Asplund, M. C.; Snee, P. T.; Yeston, J. S.; Wilkens, M. J.; Payne, C. K.; Yang, H.; Kotz, K. T.; Frei, H.; Bergman, R. G.; Harris, C. B. Ultrafast UV Pump/IR Probe Studies of C-H Activation in Linear, Cyclic, and Aryl Hydrocarbons. *J. Am. Chem. Soc.* **2002**, *124*, 10605-10612.
- (25) Guan, J.; Wriglesworth, A.; Sun, X. Z.; Brothers, E. N.; Zarić, S. D.; Evans, M. E.; Jones, W. D.; Towrie, M.; Hall, M. B.; George, M. W. Probing the Carbon-Hydrogen Activation of Alkanes Following Photolysis of Tp^{*}Rh(CNR)(Carbodiimide): A Computational and Time-Resolved Infrared Spectroscopic Study. *J. Am. Chem. Soc.* **2018**, *140*, 1842-1854.
- (26) Bengali, A. A.; Schultz, R. H.; Moore, C. B.; Bergman, R. G. Activation of the C-H Bonds in Neopentane and Neopentane-D₁₂ by (η^5 -C₅(CH₃)₅)Rh(CO)₂: Spectroscopic and Temporal Resolution of Rhodium-Krypton and Rhodium-Alkane Complex Intermediates. *J. Am. Chem. Soc.* **1994**, *116*, 9585-9589.
- (27) Chen, G. S.; Labinger, J. A.; Bercaw, J. E. The Role of Alkane Coordination in C-H Bond Cleavage at a Pt(II) Center. *Proc. Nat. Acad. (USA)* **2007**, *104*, 6915-6920.
- (28) Najafian, A.; Cundari, T. R. C-H Activation of Methane by Nickel-Methoxide Complexes: A Density Functional Theory Study. *Organometallics* **2018**, *37*, 3111-3121.
- (29) McNamara, B. K.; Yeston, J. S.; Bergman, R. G.; Moore, C. B. The Effect of Alkane Structure on Rates of Photoinduced C-H Bond Activation by Cp^{*}Rh(CO)₂ in Liquid Rare Gas Media: An Infrared Flash Kinetics Study. *J. Am. Chem. Soc.* **1999**, *121*, 6437-6443.
- (30) Sattler, A. Hydrogen/Deuterium (H/D) Exchange Catalysis in Alkanes. *ACS Cat.* **2018**, *8*, 2296-2312.
- (31) For intramolecular, agostic, sigma interactions alkyl dehydrogenation can be rather straightforward. See, for example: Chaplin, A. B.; Poblador-Bahamonde, A. I.; Sparkes, H. A.; Howard, J. A. K.; Macgregor, S. A.; Weller, A. S. Alkyl dehydrogenation in a Rh(I) complex via an isolated agostic intermediate *Chem. Commun.* **2009**, 244-246.
- (32) Wasserman, E. P.; Moore, C. B.; Bergman, R. G. Gas-Phase Rates of Alkane C-H Oxidative Addition to a Transient CpRh(CO) Complex. *Science* **1992**, *255*, 315-318.
- (33) Schultz, R. H.; Bengali, A. A.; Tauber, M. J.; Weiller, B. H.; Wasserman, E. P.; Kyle, K. R.; Moore, C. B.; Bergman, R. G. Ir Flash Kinetic Spectroscopy of C-H Bond Activation of Cyclohexane-D₀ and -D₁₂ by Cp^{*}Rh(CO)₂ in Liquid Rare Gases: Kinetics, Thermodynamics, and Unusual Isotope Effect. *J. Am. Chem. Soc.* **1994**, *116*, 7369-7377.
- (34) Crestani, M. G.; Hickey, A. K.; Gao, X.; Pinter, B.; Cavaliere, V. N.; Ito, J.-I.; Chen, C.-H.; Mindiola, D. J. Room Temperature Dehydrogenation of Ethane, Propane, Linear Alkanes

C4–C8, and Some Cyclic Alkanes by Titanium–Carbon Multiple Bonds. *J. Am. Chem. Soc.* **2013**, *135*, 14754–14767.

(35) Dobereiner, G. E.; Crabtree, R. H. Dehydrogenation as a Substrate-Activating Strategy in Homogeneous Transition-Metal Catalysis. *Chem. Rev.* **2010**, *110*, 681–703.

(36) Balcells, D.; Clot, E.; Eisenstein, O. C–H Bond Activation in Transition Metal Species from a Computational Perspective. *Chem. Rev.* **2010**, *110*, 749–823.

(37) Boutadla, Y.; Davies, D. L.; Macgregor, S. A.; Poblador-Bahamonde, A. I. Mechanisms of C–H Bond Activation: Rich Synergy between Computation and Experiment. *Dalton Trans.* **2009**, 5820–5831.

(38) Huang, Z.; White, P. S.; Brookhart, M. Ligand Exchanges and Selective Catalytic Hydrogenation in Molecular Single Crystals. *Nature* **2010**, *465*, 598–601.

(39) Petrosko, S. H.; Johnson, R.; White, H.; Mirkin, C. A. Nanoreactors: Small Spaces, Big Implications in Chemistry. *J. Am. Chem. Soc.* **2016**, *138*, 7443–7445.

(40) Pike, S. D.; Thompson, A. L.; Algarra, A. G.; Apperley, D. C.; Macgregor, S. A.; Weller, A. S. Synthesis and Characterization of a Rhodium(I) σ -Alkane Complex in the Solid State. *Science* **2012**, *337*, 1648–1651.

(41) Pike, S. D.; Chadwick, F. M.; Rees, N. H.; Scott, M. P.; Weller, A. S.; Krämer, T.; Macgregor, S. A. Solid-State Synthesis and Characterization of σ -Alkane Complexes, $[\text{Rh}(\text{L}_2)(\eta^2, \eta^2\text{-C}_7\text{H}_{12})][\text{BAR}^{\text{F}}_4]$ (L_2 = Bidentate Chelating Phosphine). *J. Am. Chem. Soc.* **2015**, *137*, 820–833.

(42) Martínez-Martínez, A. J.; Tegner, B. E.; McKay, A. I.; Bukvic, A. J.; Rees, N. H.; Tizzard, G. J.; Coles, S. J.; Warren, M. R.; Macgregor, S. A.; Weller, A. S. Modulation of σ -Alkane Interactions in $[\text{Rh}(\text{L}_2)(\text{Alkane})]^+$ Solid-State Molecular Organometallic (Smom) Systems by Variation of the Chelating Phosphine and Alkane: Access to η^2, η^2 - σ -Alkane Rh(I), η^2 σ -Alkane Rh(III) Complexes, and Alkane Encapsulation. *J. Am. Chem. Soc.* **2018**, *140*, 14958–14970.

(43) McKay, A. I.; Krämer, T.; Rees, N. H.; Thompson, A. L.; Christensen, K. E.; Macgregor, S. A.; Weller, A. S. Formation of a Σ -Alkane Complex and a Molecular Rearrangement in the Solid-State: $[\text{Rh}(\text{C}_7\text{H}_{12}\text{CH}_2\text{CH}_2\text{PCy}_2)(\eta^2, \eta^2\text{-C}_7\text{H}_{12})][\text{BAR}^{\text{F}}_4]$. *Organometallics* **2017**, *36*, 22–25.

(44) Obenaus, F.; Droste, W.; Neumeister, J. In *Ullmann's Encyclopedia of Industrial Chemistry*; Wiley-VCH: Weinheim, 2014.

(45) Olah, G. A.; Molnár, Á.; Prakash, G. K. S. *Hydrocarbon Chemistry*; John Wiley & Sons, Inc: Hoboken, 2018.

(46) See Supporting Materials

(47) Chadwick, F. M.; McKay, A. I.; Martínez-Martínez, A. J.; Rees, N. H.; Krämer, T.; Macgregor, S. A.; Weller, A. S. Solid-State Molecular Organometallic Chemistry. Single-Crystal to Single-Crystal Reactivity and Catalysis with Light Hydrocarbon Substrates. *Chem. Sci.* **2017**, *8*, 6014–6029.

(48) Baumann, R.; Stumpf, R.; Davis, W. M.; Liang, L.-C.; Schrock, R. R. Titanium and Zirconium Complexes That Contain the Tridentate Diamido Ligands $[(\text{I-Pr}^n\text{-O-C}_6\text{H}_4)_2]^{2-}$ ($[\text{I-Pr}^n\text{-O-C}_6\text{H}_4]^{2-}$) and $[(\text{C}_6\text{H}_{11}\text{-O-C}_6\text{H}_4)_2]^{2-}$ ($[\text{Cynon}]^{2-}$). *J. Am. Chem. Soc.* **1999**, *121*, 7822–7836.

(49) Chapp, S. M.; Schley, N. D. Evidence for Reversible Cyclometalation in Alkane Dehydrogenation and C–O Bond Cleavage at Iridium Bis(Phosphine) Complexes. *Organometallics* **2017**, *36*, 4355–4358.

(50) See Supporting Materials for QTAIM, NBO and NCI plot data. A full account of the bonding in these and related alkane complexes will be the subject of a separate publication

(51) Under these conditions an intermediate is observed on the way to $[\text{I-BAR}^{\text{F}}_4]$, $\delta \sim 100$, that we have not been able to identify but propose is the initial product of alkane loss (see Fig. S14).

(52) QTAIM, NBO and NCI analyses suggest an interaction intermediate between the extremes of η^2, η^2 and η^1, η^1 (see Figures S118–120 for details)

(53) Chadwick, F. M.; Rees, N. H.; Weller, A. S.; Krämer, T.; Iannuzzi, M.; Macgregor, S. A. A Rhodium–Pentane Sigma-Alkane Complex: Characterization in the Solid State by Experimental and

Computational Techniques. *Angew. Chem. Int. Ed.* **2016**, *55*, 3677–3681.

(54) Characterized at low temperature by analogy with crystallographically characterized $[\text{Rh}(\text{Pr}_2\text{PCH}_2\text{CH}_2\text{CH}_2\text{P}^i\text{Pr}_2)(\kappa^2\text{-Cl}_2\text{C}_2\text{H}_4)][\text{BAR}^{\text{F}}_4]$. See Ref. 41

(55) Douglas, T. M.; Chaplin, A. B.; Weller, A. S. Dihydrogen Loss from a 14-Electron Rhodium(III) Bis-Phosphine Dihydride to Give a Rhodium(I) Complex That Undergoes Oxidative Addition with Aryl Chlorides. *Organometallics* **2008**, *27*, 2918–2921.

(56) Chadwick, F. M.; Krämer, T.; Gutmann, T.; Rees, N. H.; Thompson, A. L.; Edwards, A. J.; Buntkowsky, G.; Macgregor, S. A.; Weller, A. S. Selective C–H Activation at a Molecular Rhodium Sigma-Alkane Complex by Solid/Gas Single-Crystal to Single-Crystal H/D Exchange. *J. Am. Chem. Soc.* **2016**, *138*, 13369–13378.

(57) *NMR Crystallography*; Harris, R. K.; Wasylishen, R. E.; Duer, M. J., Eds.; John Wiley & Sons: Chichester, 2009.

(58) Methylene groups C4 and C6 and each show one relatively close H \cdots arene centroid distance 3.0 and 2.7 Å similar to $[\text{I-NBA}][\text{BAR}^{\text{F}}_4]$.

(59) Smart, K. A.; Grellier, M.; Coppel, Y.; Vendier, L.; Mason, S. A.; Capelli, S. C.; Albinati, A.; Montiel-Palma, V.; Muñoz-Hernández, M. A.; Sabo-Étienne, S. Nature of Si–H Interactions in a Series of Ruthenium Silazane Complexes Using Multinuclear Solid-State NMR and Neutron Diffraction. *Inorg. Chem.* **2014**, *53*, 1156–1165.

(60) Lawes, D. J.; Darwish, T. A.; Clark, T.; Harper, J. B.; Ball, G. E. A Rhenium–Cyclohexane Complex with Preferential Binding of Axial C–H Bonds: A Probe into the Relative Ability of C–H, C–D, and C–C Bonds as Hyperconjugative Electron Donors? *Angew. Chem. Int. Ed.* **2006**, *45*, 4486–4490.

(61) Torres, O.; Calladine, J. A.; Duckett, S. B.; George, M. W.; Perutz, R. N. Detection of σ -Alkane Complexes of Manganese by Nmr and Ir Spectroscopy in Solution: $(\eta^5\text{-C}_5\text{H}_5)\text{Mn}(\text{CO})$ (Ethane) and $(\eta^5\text{-C}_5\text{H}_5)\text{Mn}(\text{CO})$ (Isopentane). *Chem. Sci.* **2015**, *6*, 418–424.

(62) Pitts, A. L.; Wriglesworth, A.; Sun, X.-Z.; Calladine, J. A.; Zarić, S. D.; George, M. W.; Hall, M. B. Carbon–Hydrogen Activation of Cycloalkanes by Cyclopentadienylcarbonylrhodium—a Lifetime Enigma. *J. Am. Chem. Soc.* **2014**, *136*, 8614–8625.

(63) Addition of D_2 to $[\text{I-C}_4\text{H}_{10}][\text{BAR}^{\text{F}}_4]$ does, however, result in D-incorporation into both methine and methyl groups.

(64) Perutz, R. N.; Sabo-Étienne, S. The σ -CAM Mechanism: σ Complexes as the Basis of σ -Bond Metathesis at Late-Transition-Metal Centers. *Angew. Chem. Int. Ed.* **2007**, *46*, 2578–2592.

(65) Hoops, S.; Sahle, S.; Gauges, R.; Lee, C.; Pahle, J.; Simus, N.; Singhal, M.; Xu, L.; Mendes, P.; Kummer, U. Copasi—a Complex Pathway Simulator. *Bioinformatics* **2006**, *22*, 3067–3074.

(66) Oliván, M.; Marchenko, A. V.; Coalter, J. N.; Caulton, K. G. Gas/Solid Reactivity of Unsaturated Ruthenium-Containing Molecular Solids. *J. Am. Chem. Soc.* **1997**, *119*, 8389–8390.

(67) Albrecht, M.; Lutz, M.; Schreurs, A. M. M.; Lutz, E. T. H.; Spek, A. L.; van Koten, G. Self-Assembled Organoplatinum(II) Supermolecules as Crystalline, SO_2 Gas-Triggered Switches. *J. Chem. Soc., Dalton Trans.* **2000**, 3797–3804.

(68) Albrecht, M.; Lutz, M.; Spek, A. L.; van Koten, G. Organoplatinum Crystals for Gas-Triggered Switches. *Nature* **2000**, *406*, 970–974.

(69) A consecutive 2nd/1st order process also fits the data, but less well than two 1st order process. However, given the lack of data points that define the first dehydrogenation we cannot rule this possibility out.

(70) Sadow, A. D.; Tilley, T. D. Homogeneous Catalysis with Methane. A Strategy for the Hydromethylation of Olefins Based on the Nondegenerate Exchange of Alkyl Groups and σ -Bond Metathesis at Scandium. *J. Am. Chem. Soc.* **2003**, *125*, 7971–7977.

(71) Bertmer, M.; Nieuwendael, R. C.; Barnes, A. B.; Hayes, S. E. Solid-State Photodimerization Kinetics of A-Trans-Cinnamic Acid to A-Truxillic Acid Studied Via Solid-State NMR. *J. Phys. Chem. B* **2006**, *110*, 6270–6273.

(72) Hulbert, S. F. Models for Solid-State Reactions in Powdered Compacts: A Review. *J. Br. Ceram. Soc.* **1969**, *6*, 11–20.

(73) Finney, E. E.; Finke, R. G. Is There a Minimal Chemical Mechanism Underlying Classical Avrami-Erofe'ev Treatments of Phase-Transformation Kinetic Data? *Chem. Mat.* **2009**, *21*, 4692-4705.

(74) Khawam, A.; Flanagan, D. R. Solid-State Kinetic Models: Basics and Mathematical Fundamentals. *J. Phys. Chem. B* **2006**, *110*, 17315-17328.

(75) Benedict, J. B.; Coppens, P. Kinetics of the Single-Crystal to Single-Crystal Two-Photon Photodimerization of A-Trans-Cinnamic Acid to A-Truxillic Acid. *J. Phys. Chem. A* **2009**, *113*, 3116-3120.

(76) Jarvis, A. G.; Sparkes, H. A.; Tallentire, S. E.; Hatcher, L. E.; Warren, M. R.; Raithby, P. R.; Allan, D. R.; Whitwood, A. C.; Cockett, M. C. R.; Duckett, S. B.; Clark, J. L.; Fairlamb, I. J. S. Photochemical-Mediated Solid-State [2+2]-Cycloaddition Reactions of an Unsymmetrical Dibenzylidene Acetone (Monothiophos-DBa). *CrystEngComm* **2012**, *14*, 5564-5571.

(77) Hatcher, L. E.; Skelton, J. M.; Warren, M. R.; Stubbs, C.; da Silva, E. L.; Raithby, P. R. Monitoring Photo-Induced Population Dynamics in Metastable Linkage Isomer Crystals: A Crystallographic Kinetic Study of [Pd(Bu₄dien)NO₂]BPh₄. *Phys. Chem. Chem. Phys.* **2018**, *20*, 5874-5886.

(78) Pike, S. D.; Krämer, T.; Rees, N. H.; Macgregor, S. A.; Weller, A. S. Stoichiometric and Catalytic Solid-Gas Reactivity of Rhodium Bis-Phosphine Complexes. *Organometallics* **2015**, *34*, 1487-1497.

(79) Under this constraint there are two structures that can be generated depending on which C-C is dehydrogenated. The more stable option is used here and details of the alternative structure are provided in the Supporting Materials.

(80) The alternative pathway based on initial C-H³ bond activation has a slightly larger barrier of 23.9 kcal/mol and is generally somewhat less accessible than the pathway in Figure 7. This reflects the asymmetry of the cyclohexane binding pocket which renders the C-H¹ and C-H³ bonds inequivalent. Full details of this alternative pathway are in the Supporting Materials

(81) A geometry for **VI** in which H₂ was retained in the lattice was also derived from the characterisation of **TS(V-VI)**. This had a free energy of +9.7 kcal/mol and had essentially the same coordination geometry around Rh. The drop in free energy to +2.8 kcal/mol reflects the entropy gain upon releasing free gaseous H₂. See Supporting Materials for details, Figure S101.

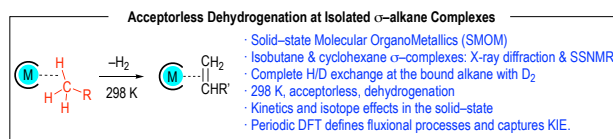
(82) This value differs from ΔG^{Rh} (+6.3 kcal/mol) as the two models employed are not the same: here one Rh-cyclohexene moiety is computed in the presence of three Rh-cyclohexane cations (and four [BARF₄]⁻ anions), whereas ΔG^{Rh} is based on dehydrogenation of all four Rh centers

(83) An alternative pathway based on the initial formation of an *endo*-Rh-H/allyl intermediate, a trans-cis isomerisation prior to H₂ loss was ruled out on the basis of calculations on the isolated cation that indicated a high energy isomerisation process. See Supporting Materials for details, Figure S100.

(84) A related transition state at +16.5 kcal/mol involves counter-clockwise rotation of the cyclohexane and generates a 2,6-structure that is geometrically equivalent to the initial 1,3-chair. (Supporting Materials, Figure S107).

(85) Kumar, A.; Zhou, T.; Emge, T. J.; Mironov, O.; Saxton, R. J.; Krogh-Jespersen, K.; Goldman, A. S. Dehydrogenation of N-Alkanes by Solid-Phase Molecular Pincer-Iridium Catalysts. High Yields of A-Olefin Product. *J. Am. Chem. Soc.* **2015**, *137*, 9894-9911.

(86) Boris Sheludko, B.; Cunningham, M.T.; Goldman, A. S.; Celik, F. E. Continuous-Flow Alkane Dehydrogenation by Supported Pincer-Ligated Iridium Catalysts at Elevated Temperatures *ACS Catal.* **2018**, *8*, 7828-7841



ToC
